

ARTICLE OPEN

Synthesis of layered platelets by self-assembly of rhenium-based clusters directed by long-chain amines

Andrés Seral-Ascaso^{1,2}, Clive Downing¹, Hannah C. Nerl^{1,2}, Anuj Pokle^{1,2}, Sonia Metel¹, Joao Coelho^{1,3}, Nina C. Berner^{1,3}, Andrew Harvey^{1,2}, Karsten Rode^{1,2}, Manuel Ruether^{1,3}, Owen Hickey^{2,3}, Georg Duesberg^{1,3}, Jonathan Coleman^{1,2} and Valeria Nicolosi^{1,2,3}

Self-assembly of nanomaterials by wet chemistry methods is a suitable approach for the preparation of engineered structures with novel functionalities. In this work, we study the ability of long-chain amines to direct the growth of a layered nanomaterial, using $[\text{Re}_x\text{Se}_y\text{Cl}_z]$ clusters as building blocks. The amines link to the clusters as ligands during the synthesis, directing the self-assembly due to their amphiphilic properties, which produces a platelet-shaped 2D material with sizes up to several μm in diameter and thicknesses in the range of 60–80 nm. This is, to the best of our knowledge, the first report on a one-step mild chemistry method for the preparation of 2D structures composed of alternate layers of self-assembled amines and sub-nm clusters of a rhenium chalcogenide. Furthermore, these materials can be used as a suitable source of clusters which then, conveniently released by a simple acid/base reaction, have been successfully incorporated to the surface of graphene. The simple clusters deposition method developed here offers a promising route towards the preparation of hybrid clusters/2D materials with outstanding properties arising from quantum confinement effects combined with high surface areas and the enormous compositional variety of 2D materials and clusters. These hybrids are expected to play a key role in the development of active materials for applications ranging from highly efficient energy storage systems, more active catalysts and upper-sensitivity gas sensors.

npj 2D Materials and Applications (2017)1:11; doi:10.1038/s41699-017-0015-5

INTRODUCTION

Two-dimensional (2D) materials have emerged as promising candidates for a broad range of applications, which include energy storage,^{1–4} catalyst supports,^{5, 6} transistors^{1, 4, 7, 8} or drug delivery agents.^{9, 10} There has been intense research to define suitable routes for the production of ultrathin nanosheets of layered materials, based either on the exfoliation of the bulk compounds by different techniques^{4, 11–17} or on the growth of the 2D materials from molecular precursors via chemical vapour deposition^{18, 19} and wet chemistry methods.^{4, 20} The latter is a convenient approach to obtain stable, self-standing 2D structures, due to the mild reaction conditions and the great versatility of the technique, which has been successfully applied to the synthesis of transition metal chalcogenides,^{21–23} layered double hydroxides^{24, 25} or metal oxides,^{26–28} among others. The synthesis of oxides and hydroxides by wet chemistry methods usually takes place within an aqueous medium, while the synthesis of chalcogenides usually requires the use of inert atmosphere and organic solvents, usually amphiphilic molecules (those composed of a non-polar hydrocarbon chain and a polar functional group, such as amine, carboxylic acid, alcohol or thiol) to avoid oxidation during synthesis.

The use of amphiphilic molecules presents several advantages due to their ability to direct or template the growth of nanostructures,²⁹ since the polar functional group of the amphiphile tends to interact with the growing structure while the non-polar tails interact with each other outward.^{23, 30} This

results in the stabilisation of the final structure, avoiding agglomeration and simplifying the further processing, besides that in some cases the amphiphilic molecules also become part of the structure, acting as a scaffold.^{31, 32} For example, dodecanethiol has been successfully utilised for the synthesis of size-monodisperse gold nanoparticles,³³ while long-chain amines successfully templated the growth of nanotubes of vanadium oxide³⁴ or gallium chalcogenides,³⁵ and a mixture of polymers and alcohols was used to template the growth of ultrathin 2D nanostructures of metal oxides, which do not have a layered structure in their bulk form.²⁸ In a recent report, the size and the number of layers of 2D MSe_2 (M: Mo, W) were effectively controlled through the different interactions of the growing MSe_2 structure with the functional group of the amphiphilic solvent (oleylamine, oleic acid or oleyl alcohol).³¹ Moreover, single-layer thin-films of nanoparticles with diameters below 5 nm arranged by self-assembly have also been reported in the pioneer works of Pileni et al.^{36–38}

In this work, we explore the ability of amphiphiles (long-chain amines) to template the growth of a layered, hybrid material composed of sub-nm clusters of rhenium selenide and arranged in alternate layers of clusters/amines to produce self-assembled circular platelets with diameters up to several μm and thicknesses in the range of 60–80 nm. The synthesis of the material is performed by a wet-chemistry method involving a mixture of hexadecylamine and dodecylamine as a solvent, at relatively mild reaction conditions (240 °C for 1 h). The rhenium (V) chloride

¹CRANN & AMBER, Trinity College Dublin, Dublin, Ireland; ²School of Physics, Trinity College Dublin, Dublin, Ireland and ³School of Chemistry, Trinity College Dublin, Dublin, Ireland

Correspondence: Andrés Seral-Ascaso (seralaa@tcd.ie) or Valeria Nicolosi (nicolov@tcd.ie)

Received: 12 December 2016 Revised: 20 April 2017 Accepted: 28 April 2017

Published online: 29 May 2017

($\text{Re}_2\text{Cl}_{10}$) and diphenyldiselenide (Ph_2Se_2) used as precursors decompose under these conditions to produce rhenium selenide clusters stabilized by the amines and additional chloride ligands, which self-assemble in the described hybrid structure as a result of the tail-tail interaction of the amphiphiles. Moreover, these hybrid platelets have been used as a source of clusters, which were further deposited on top of graphene. The incorporation of clusters on top of nanomaterials is a promising strategy for the development of new functionalities with fascinating potential for the development of novel applications in photonics, energy harvesting or catalysis.^{39, 40}

RESULTS AND DISCUSSION

Characterisation of the platelets

Scanning electron microscopy (SEM) shows that the material is composed of platelet-like particles with a circular shape and diameters in the range of 0.5–2 μm (usually around 1 μm), which sometimes present a wrinkled or folded surface and conform to the topography of the substrate as a result of their high flexibility (Fig. 1a, b). These platelets have a layered nature, which is observed due to the arising of electron-charged brighter areas at the edge of the layers since the sample is non-conductive (*inset* in Fig. 1a). The particles can be easily dispersed in isopropyl alcohol (IPA) by mild sonication, although an excess of sonication power or time may lead to the particle breaking in smaller, irregular pieces. The thickness of the particles, studied by atomic force microscopy (AFM), shows values between 60 and 80 nm, and steps are usually observed at the top surface of the platelets, with a value multiple of ~ 3.1 nm, which is the smallest observed step (Fig. 1c, d).

High-angle annular dark-field (HAADF) scanning transmission electron microscopy (STEM) of a region, which has a fold parallel to the electron beam confirms that the material is composed of superimposed layers (Fig. 2a), while the analysis of a flat edge reveals their granular nature (Fig. 2b). Interestingly, these granules consist of clusters of atoms with a variable morphology: most of them present a *diamond (rhombus)* shape, which resemble the clusters observed in ReQ_2 ($\text{Q} = \text{S}, \text{Se}$),^{41–43} while other structures,

such as *triangles* or *polyhedrons* are also observed (Fig. 2b–d and Supplementary Fig. S1 in Electronic supplementary material (ESM)).

The rhenium atoms appear as *bright spots* in the images and selenium is probably seen with much smaller contrast as *blurry spots*, while the lighter elements (carbon, nitrogen, chlorine) are not seen due to the small contrast caused by their small atomic number with respect to the rhenium. The rhenium–rhenium distances in the clusters were measured by acquiring 30 intensity profiles and the distribution of the bond length (which are in the range of 0.175–0.300 \AA) is displayed as an *inset* in the Supplementary Fig. S1 in ESM. The homogeneous distribution of both rhenium and selenium in the sample was confirmed by energy-dispersive X-ray spectroscopy (EDX) mapping performed in the STEM microscope (Fig. 2e).

The synthesis of nanomaterials by using wet chemistry methods usually proceeds via LaMer Theory (nucleation from the molecular precursors + growth). In this work, the usual metastable step of formation of clusters, which further evolve to nanosheets, as observed for cadmium (II) selenide²³ seems to have been stabilized by the presence of the long-chain amines and the obtained platelets are composed by clusters instead of sheets.

X-ray diffraction (XRD) of the sample, displayed in Fig. 3a in the d-spacing scale, indicates that the sample has a low crystallinity and shows a weak, broad band between d-spacing of 1.7 to 3 \AA , in the same order of magnitude as the rhenium–rhenium distances measured by STEM (*inset* in Fig. 3a), which is probably due to the overlapping of low intensity peaks, arising from the interatomic distances in the clusters. The ability of rhenium to form chalcogenide compounds which contains rhenium–rhenium single or multiple bonds has led to the report of a variety of structures, which includes triangular-shaped clusters of the type $[\text{Re}_3\text{Q}_7\text{Cl}_6]\text{Cl}$ ($\text{Q} = \text{S}, \text{Se}$),⁴⁴ tetrahedral and rhomboidal clusters like $[\text{Re}_4\text{Se}_4(\text{S}_3)_4(\text{S}_4)_2]^{4-}$ and $[\text{Re}_4\text{S}_2(\text{SO}_4)_4(\text{CN}_{10})^{8-}$ (ref. 41, 43), and cluster complexes which contain the octahedral core $[\text{Re}_6\text{Q}_8]$ ($\text{Q} = \text{S}, \text{Se}$).^{45–48} In the rhenium chalcogenide clusters, the rhenium–rhenium distances are in the range of 2.60 to 3.40 \AA , while the rhenium–selenium distances are around 2.5 \AA .^{41, 44, 47, 49} In the clusters reported in this work, the rhenium–rhenium

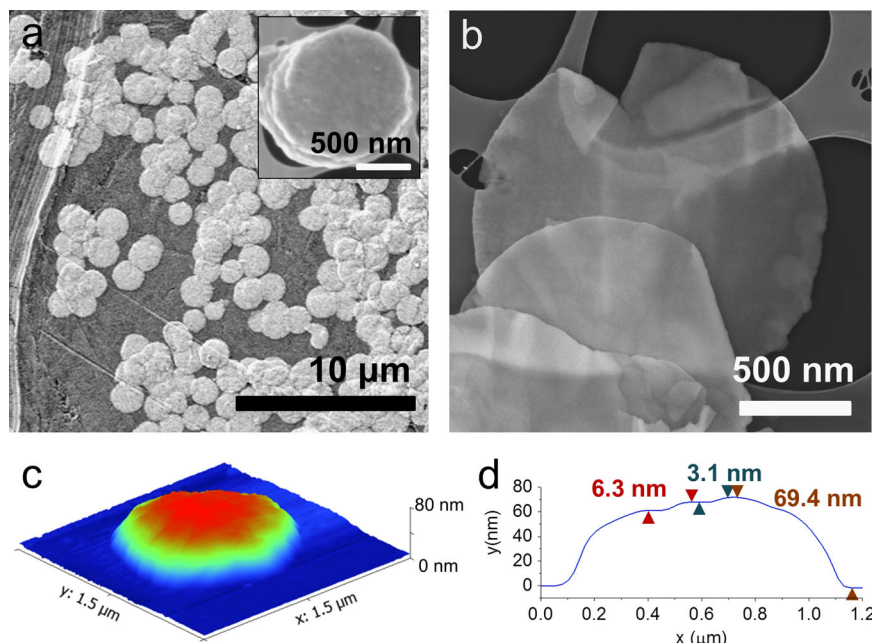


Fig. 1 SEM images of platelet-like particles on top of a substrate (**a**) and on top of a TEM grid (**b**) and *inset* in **a**. AFM 3D image of a single platelet (**c**). The thickness profile at the centre of the platelet is displayed in **d**: the measured thickness is 69.4 nm and several steps are observed on top, the smallest measured step has a value of 3.1 nm

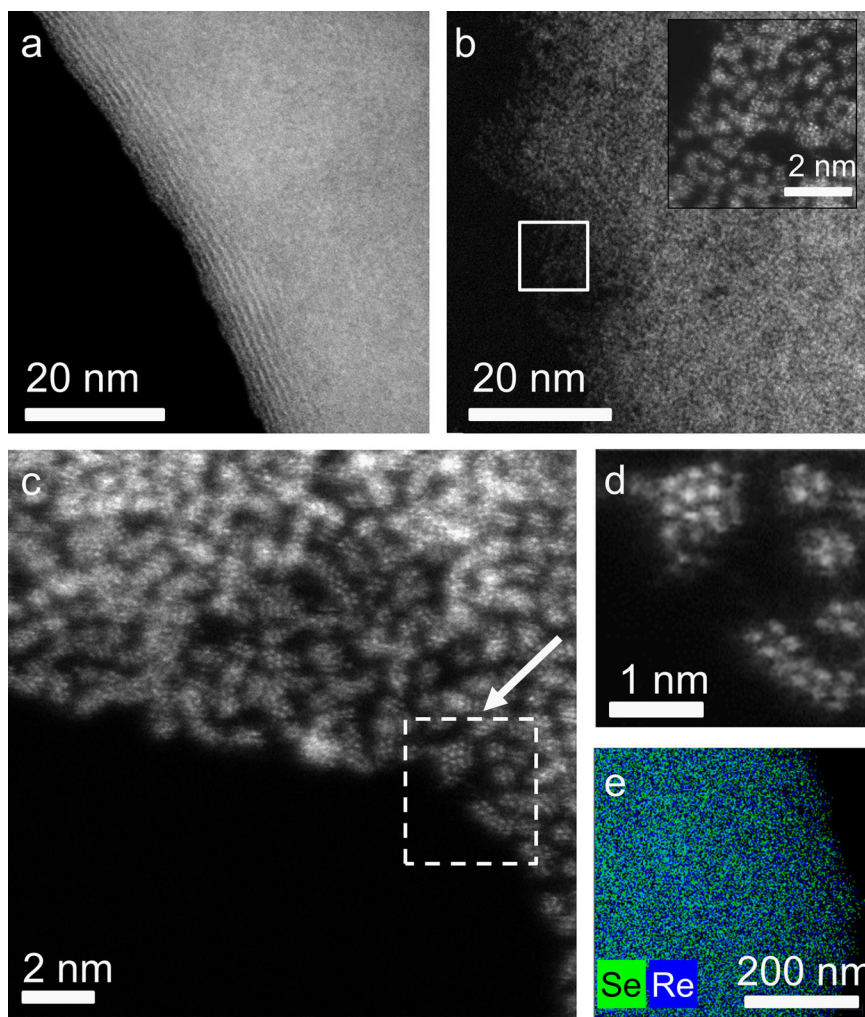


Fig. 2 HAADF-STEM images of the platelets showing the layers of an edge, which is folded parallel to the beam (**a**) and the clusters that make up the layers (**b–d**) and *inset* in **b**. An EDX mapping of the platelets showing the homogeneous distribution of both rhenium and selenium in the platelets, is shown in **e**

measured distances (0.175–0.300 Å) indicate a direct bonding between rhenium atoms.^{41, 49}

The main features of the XRD pattern, a series of peaks of decreasing intensity observed in the region between 6 and 18 Å, are due to the harmonics of the 00l reflection resulting from the spacing between the clusters layers. The distance between layers was calculated from these peaks, yielding a value of 30.3 Å, similar to the step distances measured by AFM and also in good agreement with the interlayer spacing found in other materials which contain long-chain amines between layers.^{35, 50, 51}

A comparison of the fourier-transform infrared (FTIR) spectra of the platelets and the long-chain amines confirms the presence of the latter in the nanostructures (Fig. 3b). The vibration frequencies involving the amino group (labelled with a *star*) appear at lower wavenumber in the platelets due to the combined effect of the interaction with the clusters through the amino group combined with the partial protonation of the amine, while the frequencies ascribed to the hydrocarbon chain (labelled with a *square*) appear at the same frequencies in both the platelets and the neat amines.^{52, 53} There is an appreciable degree of protonation of the amines in the platelets, which arises from a broad, weak band in the region between 3300 and 2000 cm⁻¹, which is overlapped with a fine structure, and a broad peak at 1600 cm⁻¹ characteristic of protonated primary amines⁵⁴ (labelled with a circle).

The X-ray photoelectron spectroscopy (XPS) survey spectrum of the platelets, shown in Fig. 3c, confirms the presence of the expected elements rhenium, selenium, carbon, nitrogen, chlorine and also a small oxygen peak, which might be due to the incorporation of small amounts of oxygen during sample post treatment. The incorporation of oxygen in the platelets as hydroxyl ligand or adsorbed moisture is consistent with the presence of a broad band at wavenumber > 3300 cm⁻¹ in the FTIR spectrum.

The XPS regions of N 1s, Re 4f and Se 3d were acquired at high resolution for a better understanding of the chemical bonding of these elements in the clusters (Fig. 3d, e). The nitrogen peak is centred at binding energies typical of amines (399.9 eV), and also, in good agreement with FTIR results, shows a contribution from protonated amines (401.5 eV). The comparison of the area of both peaks allowed the estimation of the degree of protonation of the amines as 20%, while the non-protonated amine is the remaining 80%. The presence of these positively charged molecules suggests that, similarly as described for many other [Re_xSe_yCl_z] clusters, the clusters present in the platelets might have a negative charge, which may be compensated with the protonated amines.

The selenium peak was fitted with two doublets with binding energies of 54.79 and 55.63 eV, which correspond with the 3d_{5/2} and Se 3d_{3/2} peaks, respectively. The position of the Se 3d peak is

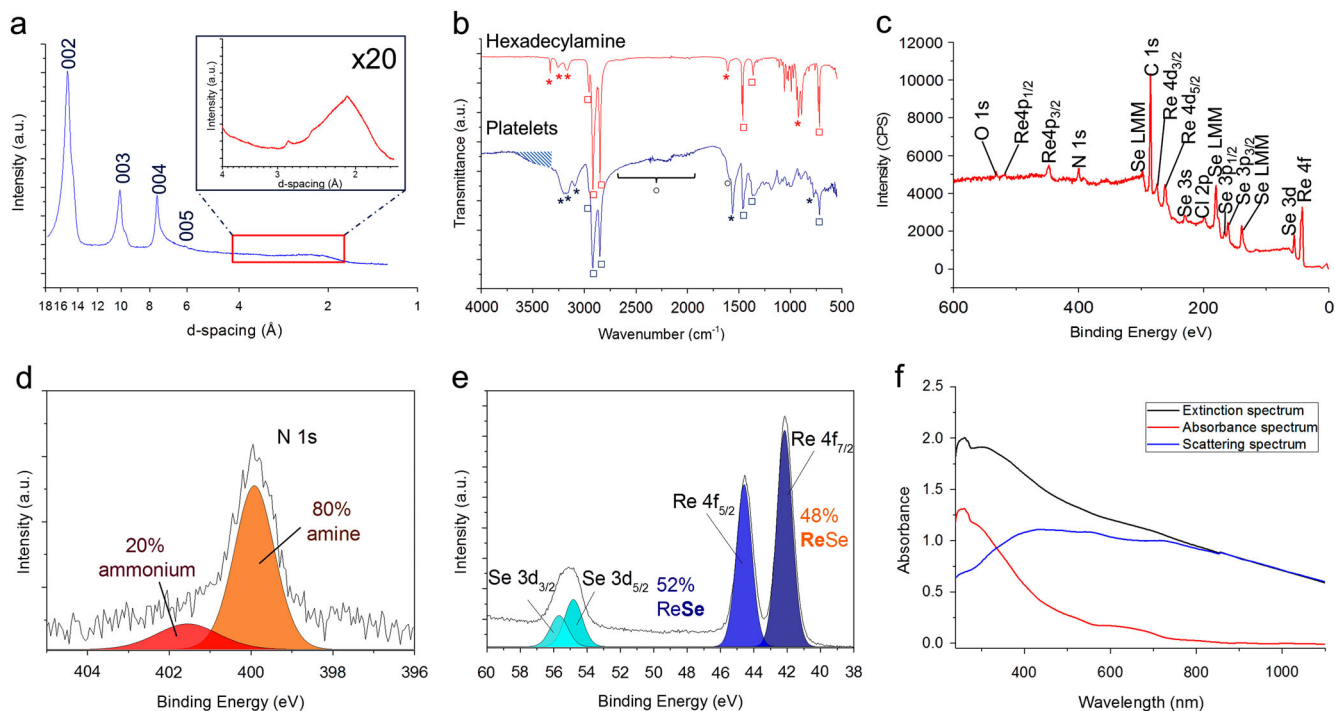


Fig. 3 XRD pattern of the platelets (**a**), FTIR comparison of neat amines and platelets (**b**), XPS survey (**c**) and XPS regions of N 1s (**d**), Se 3d and Re 4f (**e**) acquired at high resolution and UV-vis spectrum of the platelets dispersed in IPA (**f**)

similar in energies to that observed in $[\text{Re}_6\text{Se}_8]$ clusters.⁵⁵ Selenium in different environments, such as elemental selenium (55.4 eV) or selenium/oxygen species (59.1–61.0 eV) would produce chemical shifts that are not observed in the spectrum, which indicates that selenium is effectively bonded to the rhenium atoms in the clusters. The rhenium 4f peaks were also fitted with two doublets at binding energies of 42.09 and 44.53 eV, for the $4f_{7/2}$ and $4f_{5/2}$ peaks, respectively. Interestingly, the shape of both peaks is symmetric, which is usually the case for rhenium compounds but not for rhenium metal ($4f_{7/2}$ peak at 40.6 eV), which exhibits an asymmetric line profile due to significant final state effects.⁵⁶ The binding energies of the Re 4f peaks are also similar to the peaks observed in $[\text{Re}_6\text{Se}_8]$ clusters. Both Se 3d and Re 4f are shifted to higher binding energies by 0.7 eV in comparison to rhenium (IV) selenide, which could be due to the effect of charge withdrawal caused by the more electronegative chlorine atoms also chemically bonded to the rhenium clusters. Chlorine presents a peak at a binding energy of 199 eV, typical of chlorine in metal halides (198.2–199.4 eV) and similar to rhenium (III) chloride (199.4 eV). The areas of the Se 3d and Re 4f peaks were integrated in order to calculate the Se:Re atomic ratio, which yielded a value of approximately 1.08, in good agreement with the Se:Re ratio of 1.12 calculated by total X-ray fluorescence (TXRF), shown in Supplementary Fig. S2 in ESM.

Elemental analysis provided a content of 21.67% of carbon, 3.99% of hydrogen, 1.75% of nitrogen and 2.84% of chlorine in weight%, which indicates that the content of amines is approximately 27.41% in weight. Since the relative ratios between carbon, nitrogen and hydrogen are intermediate between those found in dodecylamine and hexadecylamine, probably both amines are incorporated into the platelets. Moreover, thermogravimetric analysis (TGA) in air and nitrogen atmosphere show a strong weight loss between 180 and 230 °C in both cases, probably related with the partial removal of the long-chain amines (Supplementary Fig. S3 in ESM). In air, the sample keeps losing weight when the temperature is increased above 230 °C due to selenium, and remaining amines burning and rhenium oxidation,

up to 850 °C (residue: 5.65%). Under air, the rhenium is expected to form rhenium (VII) oxide, which sublimates above 360 °C.³⁹ On the other hand, the sample remains stable up to 600 °C under nitrogen atmosphere, with a weight loss of approximately 15% before that temperature, which indicates the partial amine removal by treatment of the sample at temperatures below.

We believe that the amines can display different types of interactions within the platelets structure: some of them are slightly bonded to the structure and can be removed by heating the sample above the amines boiling points (250 and 310 °C for dodecylamine and hexadecylamine, respectively), while others, which are more strongly attached, can only be removed at temperatures above 600 °C under nitrogen atmosphere, when the whole structure collapses due to the high temperature.

Ultraviolet-visible (UV-vis) photometry of a dispersion of the platelets in IPA acquired with a standard spectrophotometer showed a strong absorption in the whole measured range (extinction spectrum, *black line* in the Fig. 3f). However, since the particles have diameters in the micron scale, a strong contribution from light scattering to the total light absorption (extinction spectrum) is expected.^{57, 58} In order to distinguish between the contributions of both absorbance and scattering to the extinction spectrum, the absorbance was measured in a spectrophotometer equipped with an integration sphere⁵⁷ (*red line* in Fig. 3f). The strong contribution arising from the scattering can be calculated by subtracting the absorbance to the extinction spectrum, and is displayed as the *blue line* in Fig. 3f. The absorbance spectrum is similar to the spectra of hexanuclear $[\text{Re}_6\text{Se}_y\text{Cl}_n]$ clusters, although shifted to higher wavelengths,⁴⁷ showing a strong absorption in the ultraviolet region, with a local maximum at 256 nm and a broad band centred at 635 nm.

Dissolution of the platelets and clusters releasing

In order to explore the possibility of processing the clusters that comprise the platelets, the preparation of a stable clusters solution by a mild chemistry method was attempted. Since the protonated

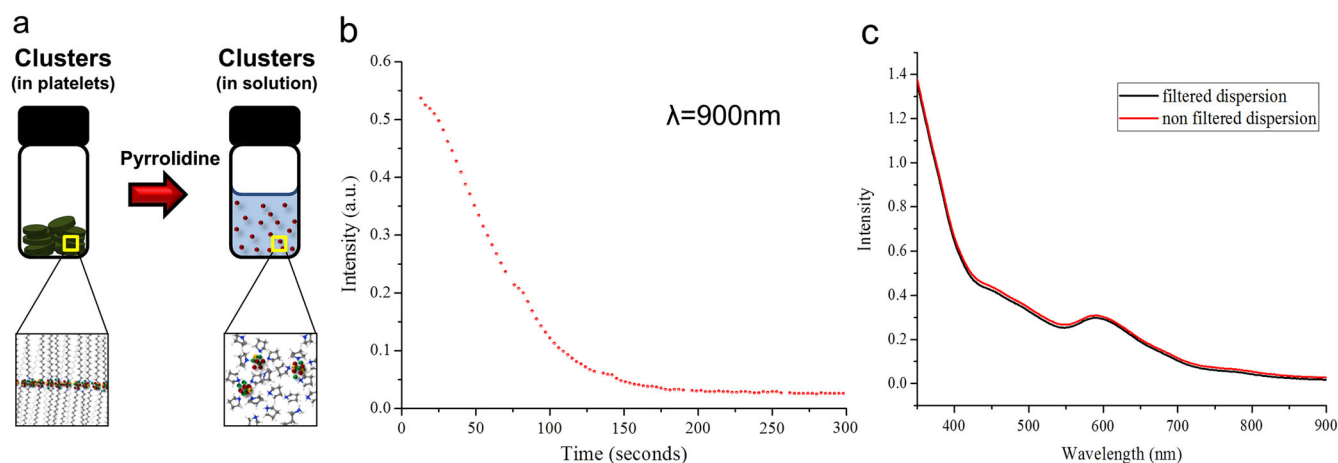


Fig. 4 Scheme of the platelets solution in pyrrolidine (a). Evolution of the intensity of the absorbed light ($\lambda = 900\text{ nm}$) with time for a mixture of platelets in IPA and pyrrolidine (b). The extinction intensity was measured every 3 s. The UV-vis spectra of the sample before and after the filtration through a filter with a pore size of 20 nm is shown in (c)

amines are expected to act as the main scaffolding to maintain the structure of the platelets, a simple treatment of the platelets with amines more basic than hexadecylamine and dodecylamine should be a suitable route to release the clusters via a simple acid–base proton exchange (Fig. 4a). For this purpose the platelets, whose primary amines have an acidity constant ($\text{p}K_a$) of 10.63, were reacted with pyrrolidine, a cyclic, secondary amine with a $\text{p}K_a$ of 11.27, which led to a quick dissolution of the same, thus producing a green solution (experimental details are described in Methods).

The dissolution kinetics was followed by UV-vis spectrophotometry, by measuring the light absorption at a fixed wavelength of 900 nm in a conventional UV-vis spectrophotometer (without the use of an integrating sphere). As mentioned before, when no integration sphere is used, both scattering (directly related to the size of the platelets) and absorbance contributes to the extinction spectra. Therefore, the measurements were carried out at 900 nm since the contribution from scattering is maximum compared to absorbance at that wavelength (see Fig. 3f). The intensity of the absorbed light at 900 nm decreased exponentially during 180 s due to the fading of the scattering contribution until reaching a residual value (due to the intrinsic absorbance of the clusters), which indicates the complete solution of the platelets elapsed that time.

After the dissolution, the mixture was further vacuum-filtered through an alumina filter (pore size 20 nm). The extinction spectra of the solution before and after the filtration (Fig. 4c) are similar, which indicates the effective solution of the materials, showing only a decrease in the intensity of the absorbed light of 3% after filtration. Moreover, the extinction spectrum of the filtered solution is also similar to the absorbance spectrum of the platelets previously described in Fig. 3f, although with the bands slightly blue-shifted, which might be due to a small solvatochromic effect.

Deposition of the clusters on top of graphene

The clusters were subsequently deposited on top of graphene by means of the destabilization of the clusters solution through the addition of a certain solvent (experimental details are described in Methods). Different solvents (water, methanol, IPA, acetone, ethoxyethane or cyclohexane) were added dropwise to a stable dispersion of clusters and graphene dispersed in a mixture of IPA and pyrrolidine (Fig. 5a). The addition of a third solvent with different polarity is expected to cause a certain destabilization of the clusters, which might either deposit on top of the graphene (as observed for acetone, ethoxyethane or cyclohexane, shown in

Fig. 5b–d) or agglomerate and precipitate (as observed when protic solvents such as water, methanol or extra IPA are used, shown in Fig. 5e–g). EDX point analysis performed at the SEM showed the presence of carbon, rhenium, selenium, chlorine, nitrogen and oxygen in all samples. As an example, the point EDX analysis on top of a graphene flake in the sample prepared with acetone (the analysed area is labelled with a yellow circle in Fig. 5b) is displayed in Supplementary Fig. S4 in ESM. Furthermore, the samples prepared using acetone, ethoxyethane and cyclohexane showed a homogenous distribution of clusters on top of the graphene flakes under low resolution transmission electron microscope (TEM, Fig. 5h–j). It must be mentioned here that the starting clusters/graphene weight ratio is 1:1, so it is not expected that all the clusters are able to deposit on top of the graphene and some probably remain in solution or precipitate afterwards. However, the optimisation of the coating process is out of the scope of the present work and will be reported in the near future.

HAADF-STEM images of the sample prepared with acetone show the clusters, with a similar morphology as in the platelets, broadly distributed on the surface of graphene (Fig. 6a, b). The EDX mapping performed at the STEM microscope (Fig. 6c–h) confirms that the clusters are composed of the same elements as in the platelets (rhenium, selenium, chlorine). The nitrogen distribution, which matches the same distribution as the clusters, indicates that, as expected, the amines (most probably, protonated pyrrolidine) are attached to them. These results confirm that this procedure is a successful method for the preparation of hybrid graphene/clusters materials.

CONCLUSIONS

This work explored the versatility of wet chemistry methods for the synthesis of hybrid 2D materials composed of metal-chalcogenide clusters and amphiphilic molecules, which act as templating agents for the growth of the structure. We report the synthesis of platelets composed of alternate layers of clusters of $[\text{Re}_x\text{Se}_y\text{Cl}_z]$ and long-chain amines, with sizes up to $2\ \mu\text{m}$ and thicknesses in the range of 60–80 nm. These materials can be easily dispersed in IPA by mild sonication and processed to produce a clusters solution by dissolving the platelets in pyrrolidine by a simple acid–base reaction. Moreover, the clusters have been deposited on top of graphene by an easy wet chemistry process, which consist in the addition of a certain solvent (acetone, ethoxyethane or cyclohexane) to destabilise the clusters dispersion and drive their deposition on top of the graphene.

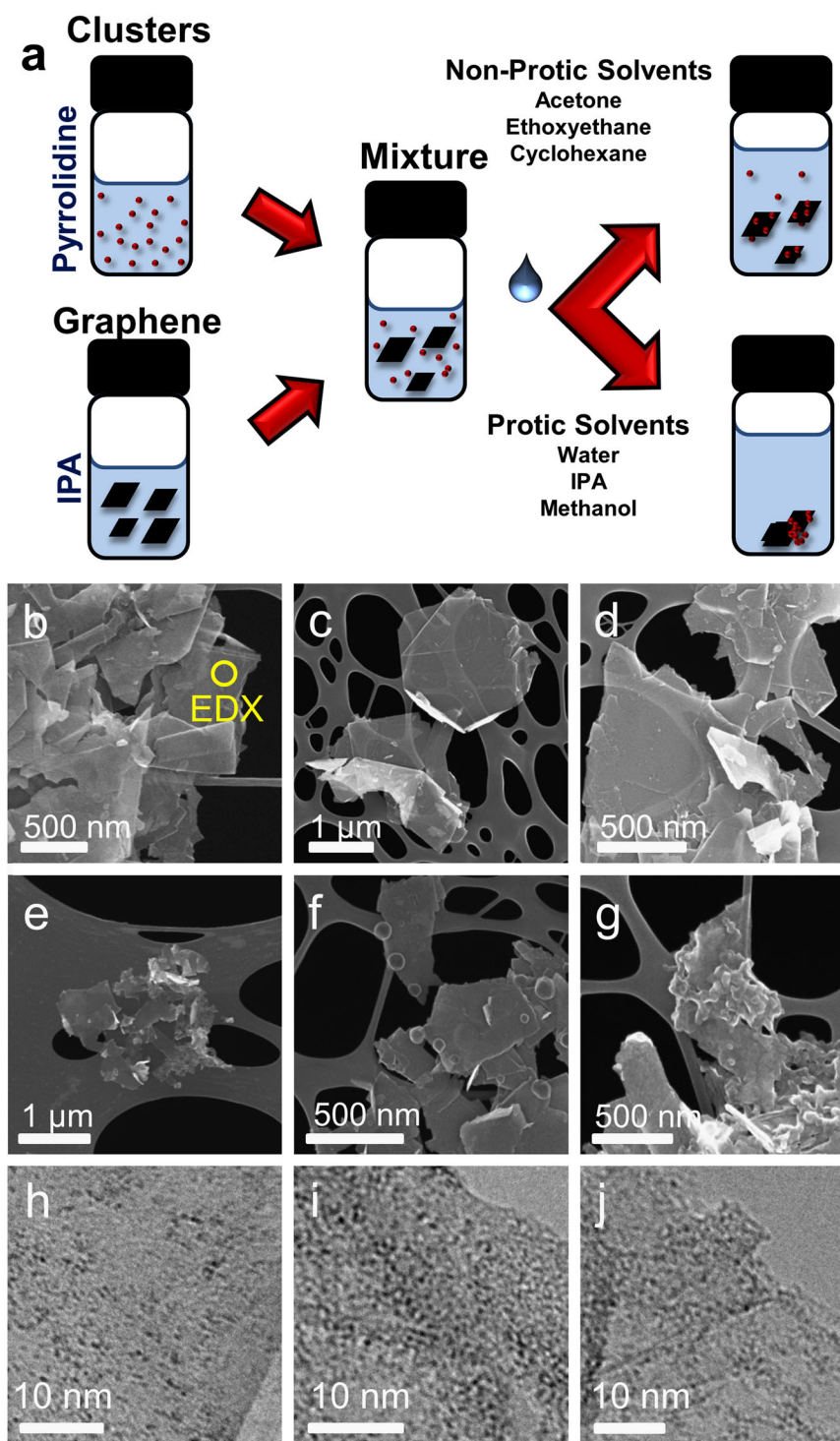


Fig. 5 Scheme of clusters deposition on top of graphene (a). SEM images of the mixtures of clusters deposited on top of graphene after the addition of acetone (b), cyclohexane (c) and ethoxyethane (d), and mixtures of graphene and agglomerated clusters produced when water (e), methanol (f) or extra IPA (g) are added. Low resolution TEM images of the clusters homogeneously distributed on top of graphene after the addition of acetone (h), cyclohexane (i) and ethoxyethane (j)

We expect that wet chemistry methods similar to the one described above are suitable routes for the synthesis of 2D materials, which incorporate clusters in their composition, by using the templating ability of long-chain amines or other amphiphilic molecules. These hybrid materials present the advantages of incorporating the properties of the clusters

together with the easy manipulation and isolation of the 2D structures, and most probably present interesting quantum confinement effects arising from its low dimensionalities. Furthermore, the simple route for clusters release and deposition here described can be probably extended to the preparation of other hybrid materials, which allows the production of a plethora of

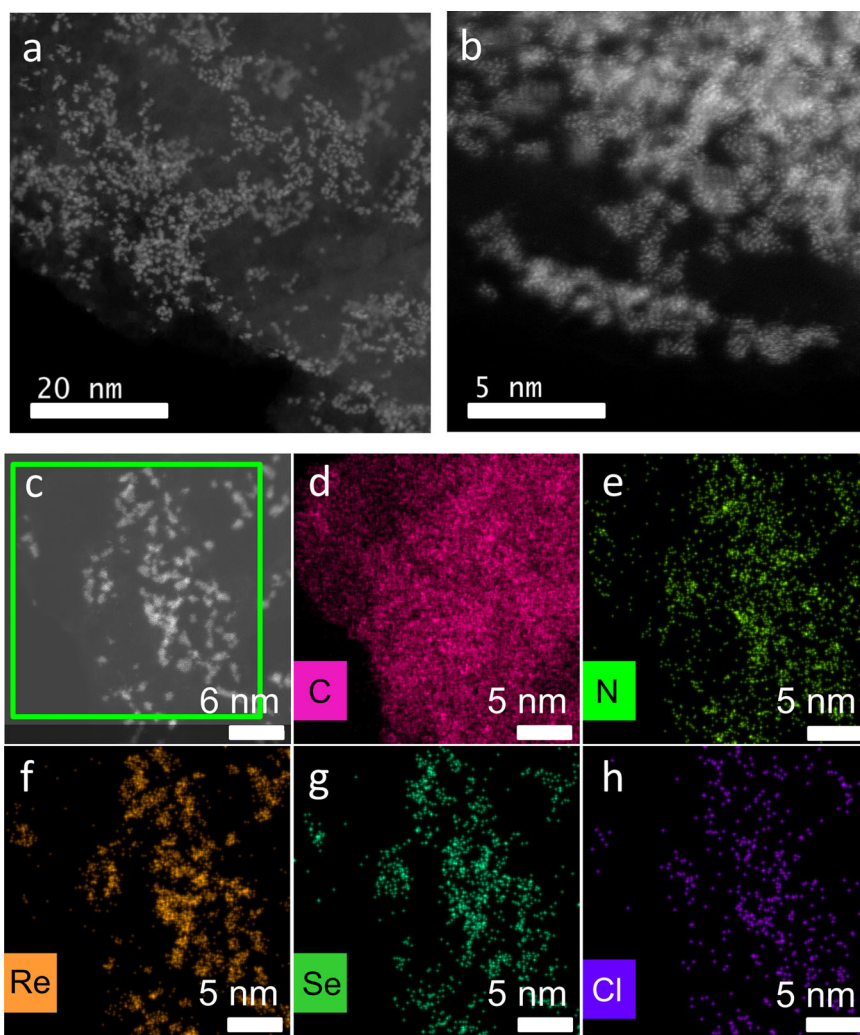


Fig. 6 HAADF STEM images of the clusters-coated graphene (**a**, **b**) and EDX mapping of a coated region, showing the overlapped position of the clusters as seen by STEM (**c**) and the carbon (**d**), nitrogen (**e**), rhenium (**f**), selenium (**g**) and chlorine (**h**) distribution

clusters/nanomaterials composites. Our future work will be focused on the developing of clusters/graphene composites as active materials for energy storage devices.

METHODS

Materials

$\text{Re}_2\text{Cl}_{10}$ (98%), Ph_2Se_2 (98%), dodecylamine (98%), hexadecylamine (technical grade, 90%), pyrrolidine (99%) acetone (anhydrous, 99%) methanol (anhydrous, 99%), IPA (anhydrous, 99%), toluene (anhydrous, 99%), ethoxyethane (anhydrous, 99%), cyclohexane (anhydrous, 99%) and graphite flakes (purity > 75%) were acquired from Sigma-Aldrich. All solvents were stored in a moisture-free atmosphere, while the $\text{Re}_2\text{Cl}_{10}$ and the Ph_2Se_2 were stored in an argon-filled glove-box until use. Graphite was used without further purification.

Synthesis of the platelets

The platelets were synthesised in a 100 cm³ two-neck flask, filled with 0.22 mmol of $\text{Re}_2\text{Cl}_{10}$ (160 mg), 0.22 mmol of Ph_2Se_2 (70 mg), 20 mmol of dodecylamine and 100 mmol of hexadecylamine, and connected to a reflux system under nitrogen atmosphere. Due to the sensitivity of $\text{Re}_2\text{Cl}_{10}$ to moisture and oxygen, the setup was handled in a way so as to avoid direct exposure to the open air.

The mixture was heated up to 60 °C under vigorous magnetic stirring until complete dissolution of the components and further heated slowly to

240 °C. This temperature was maintained for 1 h. Then, the system was allowed to cool down and 10 cm³ of toluene were added to facilitate the washing, which was performed with warm IPA (40 cm³, four times) and centrifugation.

Dissolution of the platelets and clusters releasing

Ten milligrams of the platelets were initially dissolved in 4 cm³ of pyrrolidine by hand shaking at room temperature. The solution became transparent, dark green in few minutes, indicating that the platelets were completely dissolved, whereupon it was filtered through an alumina filter with a pore size of 20 nm. A stock solution of clusters in pyrrolidine of an approximate concentration of 0.05 mg cm⁻³ was prepared by adding neat pyrrolidine to the filtered solution and labelled as solution A. N.B. to calculate the concentration, the respective long-chain amines weight (27.41% as per elemental analysis) was subtracted, and this concentration excludes the weight of pyrrolidine expected to be chemically bonded to the clusters in solution (unknown).

To measure the kinetics of the dissolution, 1.5 cm³ of pyrrolidine were added over 1.5 cm³ of platelets dispersed in IPA in a cuvette, followed by a strong hand shaking, and the light absorption was measured at a fixed wavelength of 900 nm, during 300 s, at intervals of 3 s. In order to avoid the effect of the precipitation of the platelets on the measurements, the cuvettes were hand shaken every 60 s. Consequently, the dots which correspond to the spectrophotometer openings were removed from the graph in Fig. 4a.

Deposition of the clusters on top of graphene

A stock dispersion of graphene was prepared by sonication of graphite (1 g) in 100 cm³ of IPA with a Fisher Scientific sonic tip (nominal power 500 W, working at 40% amplitude, with pulses of 5 s length for 8 h).⁹ The mixture was distributed in 50-cm³ centrifuge tubes, and centrifuged in a Heraeus Multifuge centrifuge at 3500 rpm for 90 min. Then, 30 cm³ of the supernatant of every centrifuge vial were transferred to a 200 cm³ glass bottle and the concentration of the dispersion was calculated by filtration of 20 cm³ through a polypropylene backed filter with a pore size of 0.5 μm, which resulted in 0.027 mg cm⁻³ (solution B).

A homogeneous dispersion of clusters and graphene (solution C) was produced by mixing 12 cm³ of pyrrolidine, 6 cm³ of solution A and 11.11 cm³ of solution B (slowly added), which led to a total amount of 0.3 mg of graphene and clusters, respectively, in a total volume of 29.11 cm³. At this point, no precipitation of graphene or clusters was observed, and the solution seems to be stable towards precipitation for several hours.

Then, 2 cm³ of a third solvent (water, methanol, IPA, acetone, ethoxyethane or cyclohexane) were added dropwise over 2 cm³ of solution C under vigorous stirring, and the resulting composites were characterised by SEM, EDX, TEM and HAADF-STEM.

Characterisation techniques

SEM was performed with a Zeiss Ultra Plus field-emission microscope equipped with a Gemini column (acceleration voltage 2 kV) and a secondary electron detector. Samples were prepared by mild sonication of the material in IPA and further drop casting on top of a SEM stub (Fig. 1a) and a TEM grid (Fig. 1b). HAADF-STEM images and EDX mapping were acquired using a NION Ultra STEM 200 operating at 60 kV with a Bruker windowless EDX detector. Low resolution TEM images were acquired with a JEOL USA JEM-2100Plus transmission electron microscope operated at 60 kV. AFM measurements were done in an Asylum Research MFP 3D microscope working in a tapping mode with a shift of -5%. A silicon tip coated with aluminium from Budget Sensors and a nominal resonant frequency of 300 kHz was used. The images were acquired under ambient conditions at 22 °C with a scanning rate of 1 Hz. The data were processed with Gwyddion software. A Bruker Advance Powder X-ray diffractometer equipped with a molybdenum-K α emission source ($\lambda = 0.7107 \text{ \AA}$) in the Bragg-Brentano configuration was used to acquire the XRD data, from 2θ angles of 2 to 35 degrees and with a step size of 0.01 degrees.

XPS was acquired using an Omicron XM1000 equipped with a MkII X-ray source (monochromated aluminium K α) and an Omicron EA125 energy analyser (pass energies were 15 eV for the core-level spectrum and 100 eV for the survey spectrum). Charge compensation was done with an Omicron CN10 electron flood gun. Following the subtraction of a Shirley background, the core-level spectra were fitted with Gaussian-Lorentzian line shapes with the software CasaXPS. TXRF spectrum was acquired in a S2 PicoFox TXRF spectrometer (Bruker Nano GmbH) equipped with a molybdenum X-ray source working at 600 μA at 50 kV and a XFlash SDD detector (effective area of 30 mm², energy resolution > 150 eV for manganese K α). Cobalt was used as internal standard.

The optical extinction and absorbance spectra were measured on a PerkinElmer 650 spectrometer in quartz cuvettes with a path length of 0.4 cm, from 240 to 1100 nm. The sample was dispersed in IPA by mild sonication before the measurements. The extinction spectrum was measured in the standard configuration, while the absorbance spectrum was measured using an integrator sphere, which contained the dispersion inside of a cuvette with all the sides transparent, located in the geometrical centre of the device. (N.B. the correct positioning of the cuvette is important for correct/reproducible results).⁴⁹ The scattering spectrum was calculated subtracting the absorbance to the extinction spectrum.

FTIR was acquired by the diffuse reflectance method in the range of 500–4000 cm⁻¹ using a Perkin Elmer Spectrum 100 FTIR spectrometer. TGA were carried out by heating 3.5 mg of the sample from ambient temperature to 850 °C (heating rate 10 °C min⁻¹) under air or nitrogen atmosphere, using a Perkin Elmer Pyris 1 TGA, previously calibrated with iron and nickel standards.

ACKNOWLEDGEMENTS

The authors would like to thank Carol McCaffrey and Michael Finneran from Trinity College Dublin, all the technical staff and Dr. Aleksey Shmeliov at the Advanced Microscopy Laboratory in CRANN TCD, and Ramón Fernández-Ruiz and Josué Friedrich from Universidad Autónoma de Madrid, for their support. This work was

funded through SFI/12/RC/2278, SFI AMBER, SFI PIYRA, ERC StG 2DNanoCaps, ERC PoC 2DUUSD, ERC PoC 2DInk, EU MC ITN MoWSeS, EU NMP Co-Pilot and SFI PL_10/IN.1/13030. NCB and GSD were supported by SFI PL_10/IN.1/13030.

AUTHOR CONTRIBUTIONS

A.S. and V.N. designed and discussed the project. A.S. performed the synthesis experiments, clusters solutions preparation and graphene coating experiments. A.S., S.M., J.Coelho, M.R. and O.H. performed and discussed the SEM, AFM, TEM, FTIR and TGA characterisation. C.D., N.H. and A.P. performed the HAADF-STEM and EDX mapping, N.B. and G.D. provided the XPS measurements and discussion, A.H. and J. Coleman provided the UV-vis measurements and discussion, K.R. provided assistance with the XRD measurements and discussion. A.S. and V.N. discussed the results and A.S. wrote the paper.

COMPETING INTERESTS

The authors declare that they have no competing financial interests.

REFERENCES

1. Wang, Q. H., Kalantar-Zadeh, K., Kis, A., Coleman, J. N. & Strano, M. S. Electronics and optoelectronics of two-dimensional transition metal dichalcogenides. *Nat. Nanotechnol.* **7**, 699–712 (2012).
2. Mendoza-Sanchez, B. & Gogotsi, Y. Synthesis of two-dimensional materials for capacitive energy storage. *Adv. Mater.* **28**, 6104–6135 (2016).
3. Bhandavat, R., David, L. & Singh, G. Synthesis of surface-functionalized WS₂ nanosheets and performance as Li-ion battery anodes. *J. Phys. Chem. Lett.* **3**, 1523–1530 (2012).
4. Tiwari, J. N., Tiwari, R. N. & Kim, K. S. Zero-dimensional, one-dimensional, two-dimensional and three-dimensional nanostructured materials for advanced electrochemical energy devices. *Prog. Mater. Sci.* **57**, 724–803 (2012).
5. Cano, M., Benito, A. M., Urriolabeitia, E. P., Arenal, R. & Maser, W. K. Reduced graphene oxide: Firm support for catalytically active palladium nanoparticles and game changer in selective hydrogenation reactions. *Nanoscale* **5**, 10189–10193 (2013).
6. Li, Y. J., Gao, W., Ci, L. J., Wang, C. M. & Ajayan, P. M. Catalytic performance of Pt nanoparticles on reduced graphene oxide for methanol electro-oxidation. *Carbon* **48**, 1124–1130 (2010).
7. Radisavljevic, B., Radenovic, A., Brivio, J., Giacometti, V. & Kis, A. Single-layer MoS₂ transistors. *Nat. Nanotechnol.* **6**, 147–150 (2011).
8. Buscema, M. et al. Fast and broadband photoresponse of few-layer black phosphorus field-effect transistors. *Nano Lett.* **14**, 3347–3352 (2014).
9. Sun, X. M. et al. Nano-graphene oxide for cellular imaging and drug delivery. *Nano Res.* **1**, 203–212 (2008).
10. Costantino, U., Ambrogio, V., Nocchetti, M. & Perioli, L. Hydroxalcalite-like compounds: Versatile layered hosts of molecular anions with biological activity. *Microporous Mesoporous Mater.* **107**, 149–160 (2008).
11. Hernandez, Y. et al. High-yield production of graphene by liquid-phase exfoliation of graphite. *Nat. Nanotechnol.* **3**, 563–568 (2008).
12. Coleman, J. N. et al. Two-dimensional nanosheets produced by liquid exfoliation of layered materials. *Science* **331**, 568–571 (2011).
13. Paton, K. R. et al. Scalable production of large quantities of defect-free few-layer graphene by shear exfoliation in liquids. *Nat. Mater.* **13**, 624–630 (2014).
14. Nicolosi, V., Chhowalla, M., Kanatzidis, M. G., Strano, M. S. & Coleman, J. N. Liquid exfoliation of layered materials. *Science* **340**, 1420–1454 (2013).
15. Viculis, L. M., Mack, J. J., Mayer, O. M., Hahn, H. T. & Kaner, R. B. Intercalation and exfoliation routes to graphite nanoplatelets. *J. Mater. Chem.* **15**, 974–978 (2005).
16. Joensen, P., Frindt, R. F. & Morrison, S. R. Single-layer MoS₂. *Mater. Res. Bull.* **21**, 457–461 (1986).
17. Sasaki, T., Watanabe, M., Hashizume, H., Yamada, H. & Nakazawa, H. Macromolecule-like aspects for a colloidal suspension of an exfoliated titanate. Pairwise association of nanosheets and dynamic reassembling process initiated from it. *J. Am. Chem. Soc.* **118**, 8329–8335 (1996).
18. Lee, K., Gatensby, R., McEvoy, N., Hallam, T. & Duesberg, G. S. High-performance sensors based on molybdenum disulfide thin films. *Adv. Mater.* **25**, 6699–6702 (2013).
19. Obratsov, A. N., Obratsova, E. A., Tyurnina, A. V. & Zolotukhin, A. A. Chemical vapor deposition of thin graphite films of nanometer thickness. *Carbon* **45**, 2017–2021 (2007).
20. Dou, L. T. et al. Atomically thin two-dimensional organic-inorganic hybrid perovskites. *Science* **349**, 1518–1521 (2015).

21. Altavilla, C., Sarno, M. & Ciambelli, P. A novel wet chemistry approach for the synthesis of hybrid 2D free-floating single or multilayer nanosheets of $MS_2@o$ -leylamine (M=Mo, W). *Chem. Mater.* **23**, 3879–3885 (2011).
22. Yoo, D., Kim, M., Jeong, S., Han, J. & Cheon, J. Chemical synthetic strategy for single-layer transition-metal chalcogenides. *J. Am. Chem. Soc.* **136**, 14670–14673 (2014).
23. Nasilowski, M., Mahler, B., Lhuillier, E., Ithurria, S. & Dubertret, B. Two-dimensional colloidal nanocrystals. *Chem. Rev.* **116**, 10934–10982 (2016).
24. Liu, Z. P. et al. Synthesis, anion exchange, and delamination of Co-Al layered double hydroxide: Assembly of the exfoliated nanosheet/polyanion composite films and magneto-optical studies. *J. Am. Chem. Soc.* **128**, 4872–4880 (2006).
25. Ma, R. et al. Phase transitions - Topochemical synthesis of monometallic (Co^{2+} - Co^{3+}) layered double hydroxide and its exfoliation into positively charged Co (OH)₂ nanosheets. *Angew. Chem. Int. Ed.* **47**, 86–89 (2008).
26. Lim, C. S., Sofer, Z., Jankovsky, O., Wang, H. & Pumera, M. Electrochemical properties of layered SnO and PbO for energy applications. *RSC Adv* **5**, 101949–101958 (2015).
27. Julien, C. et al. Layered $LiNi_{0.5}Co_{0.5}O_2$ cathode materials grown by soft-chemistry via various solution methods. *Mater. Sci. Eng. B Solid* **76**, 145–155 (2000).
28. Sun, Z. Q. et al. Generalized self-assembly of scalable two-dimensional transition metal oxide nanosheets. *Nat. Commun* **5**, 3813 (2014).
29. Cademartiri, L. & Ozin, G. A. Emerging strategies for the synthesis of highly monodisperse colloidal nanostructures. *Philos. Trans R. Soc. A* **368**, 4229–4248 (2010).
30. Kim, J. S., Kim, H., Yoon, J., Heo, K. & Ree, M. Synthesis of zinc glutarates with various morphologies using an amphiphilic template and their catalytic activities in the copolymerization of carbon dioxide and propylene oxide. *J. Polym. Sci. Pol. Chem.* **43**, 4079–4088 (2005).
31. Jung, W. et al. Colloidal Synthesis of single-layer MSe_2 (M=Mo, W) nanosheets via anisotropic solution-phase growth approach. *J. Am. Chem. Soc.* **137**, 7266–7269 (2015).
32. Malgras, V. et al. Templated synthesis for nanoarchitected porous materials. *B. Chem. Soc. Jpn.* **88**, 1171–1200 (2015).
33. Brust, M., Walker, M., Bethell, D., Schiffrin, D. J. & Whyman, R. Synthesis of thiol-derivatized gold nanoparticles in a 2-phase liquid-liquid system. *J. Chem. Soc. Chem. Commun.* **7**, 801–802 (1994).
34. Spahr, M. E. et al. Redox-active nanotubes of vanadium oxide. *Angew. Chem. Int. Ed.* **37**, 1263–1265 (1998).
35. Seral-Ascaso, A. et al. Long-chain amine-templated synthesis of gallium sulfide and gallium selenide nanotubes. *Nanoscale* **8**, 11698–11706 (2016).
36. Motte, L., Billoudet, F., Lacaze, E., Douin, J. & Pileni, M. P. Self-organization into 2D and 3D superlattices of nanosized particles differing by their size. *J. Phys. Chem. B* **101**, 138–144 (1997).
37. Pileni, M. P. Nanocrystal self-assemblies: Fabrication and collective properties. *J. Phys. Chem. B* **105**, 3358–3371 (2001).
38. Pileni, M. P. Self-assembly of inorganic nanocrystals: Fabrication and collective intrinsic properties. *Accounts Chem. Res.* **40**, 685–693 (2007).
39. Ishida, T., Nagaoka, M., Akita, T. & Haruta, M. Deposition of gold clusters on porous coordination polymers by solid grinding and their catalytic activity in aerobic oxidation of alcohols. *Chem. Eur. J* **14**, 8456–8460 (2008).
40. Barthel, M. J. et al. Synthesis of highly fluorescent copper clusters using living polymer chains as combined reducing agents and ligands. *ACS Nano* **9**, 11886–11897 (2015).
41. Saito, T. Rhenium sulfide cluster chemistry. *J. Chem. Soc. Dalton* **2**, 97–105 (1999).
42. Lin, Y. C. et al. Single-layer ReS_2 : two-dimensional semiconductor with tunable in-plane anisotropy. *ACS Nano* **9**, 11249–11257 (2015).
43. Muller, A., Krickemeyer, E., Bogge, H., Ratajczak, H. & Armatage, A. A building principle of amorphous chalcogenides of transition-metals - The extrusion of the electron-rich cluster $[Re_4S_2(SO_2)_4(CN)_{10}]^{8-}$ from $\alpha-Re_2S_7$. *Angew. Chem. Int. Ed.* **33**, 770–773 (1994).
44. Beck, J. & Muller-Buschbaum, K. On chalcogenide halogenides of rhenium: Synthesis and crystal structures of the triangular clusters $Re_3E_7X_7$ (E=S, Se; X=Cl, Br). *Z. Anorg. Allg. Chem.* **625**, 1212–1216 (1999).
45. Gabriel, J. C. P., Boubekeur, K., Uriel, S. & Batail, P. Chemistry of hexanuclear rhenium chalcogenide clusters. *Chem. Rev.* **101**, 2037–2066 (2001).
46. Bohm, G., Wiegardt, K., Nuber, B. & Weiss, J. Coordination chemistry of rhenium (V), rhenium(IV), and rhenium(III) with the macrocyclic ligands 1,4,7-triazacyclononane-(L) and its N-methylated derivative (L') - Crystal-structures of $[LReCl_3]Cl$, $[L_2Re_2Cl_2(\mu-Cl)(\mu-OH)]_2 \cdot 2H_2O$, $[L_2Re_2(\mu-O)]_2 \cdot 2H_2O$, and $[L_2Re_2Cl_4(\mu-O)]ZnCl_4$ - Effect of π -donors on the Re-Re bond distance. *Inorg. Chem.* **30**, 3464–3476 (1991).
47. Long, J. R., McCarty, L. S. & Holm, R. H. A solid-state route to molecular clusters: access to the solution chemistry of $[ReQ_8]^{2+}$ (Q=S, Se) core-containing clusters via dimensional reduction. *J. Am. Chem. Soc.* **118**, 4603–4616 (1996).
48. Long, J. R., Williamson, A. S. & Holm, R. H. Dimensional reduction of ReQ_8Cl_2 (Q=S, Se)—a solid-state route to molecular $[ReQ_8]^{2+}$ core-containing clusters. *Abstr. Pap. Am. Chem. Soc.* **209**, 509-Inor (1995). (abst).
49. Fedorov, V. Y., Mironov, Y. V., Naumov, N. G., Sokolov, M. N. & Fedin, V. P. Group 5–7 metal chalcogenide clusters. *Russ. Chem. Rev.* **76**, 529–552 (2007).
50. Wortham, E., Bonnet, B., Jones, D. J., Roziere, J. & Burns, G. R. Birnessite-type manganese oxide-alkylamine mesophases obtained by intercalation and their thermal behaviour. *J. Mater. Chem.* **14**, 121–126 (2004).
51. Krumeich, F. et al. Morphology and topochemical reactions of novel vanadium oxide nanotubes. *J. Am. Chem. Soc.* **121**, 8324–8331 (1999).
52. Cooper, J. K., Franco, A. M., Gul, S., Corrado, C. & Zhang, J. Z. Characterization of primary amine capped CdSe, ZnSe, and ZnS quantum dots by FT-IR: Determination of surface bonding interaction and identification of selective desorption. *Langmuir* **27**, 8486–8493 (2011).
53. Robert M. Silverstein, F. X. W., David J. Kiemle, David L. Bryce. (eds) *Spectrometric Identification of Organic Compounds* 8th edn (Wiley, 2015).
54. Helmut Gunzler, H.-U. G. (ed) *IR Spectroscopy: An Introduction*. (Wiley-VCH, 2002).
55. Cordier, S. et al. Covalent anchoring of Re_6Se_8 cluster cores mono layers on modified n- and p-type Si(111) surfaces: effect of coverage on electronic properties. *J. Phys. Chem. C* **114**, 18622–18633 (2010).
56. J.F. Moulder, W. F. S., P.E. Sobol, K.D. Bomben. (eds) *Handbook of X-ray Photoelectron Spectroscopy* 2nd ed. (Perkin-Elmer, Physical Electronics Division, 1992).
57. Backes, C. et al. Edge and confinement effects allow in situ measurement of size and thickness of liquid-exfoliated nanosheets. *Nat. Commun.* **5**, 4576 (2014).
58. Bohren, C. F. & Huffman, D. R. (eds) *Absorption and scattering of light by small particles*. (Wiley, 2008).



Open Access This article is licensed under a Creative Commons Attribution 4.0 International License, which permits use, sharing, adaptation, distribution and reproduction in any medium or format, as long as you give appropriate credit to the original author(s) and the source, provide a link to the Creative Commons license, and indicate if changes were made. The images or other third party material in this article are included in the article's Creative Commons license, unless indicated otherwise in a credit line to the material. If material is not included in the article's Creative Commons license and your intended use is not permitted by statutory regulation or exceeds the permitted use, you will need to obtain permission directly from the copyright holder. To view a copy of this license, visit <http://creativecommons.org/licenses/by/4.0/>.

© The Author(s) 2017

Supplementary Information accompanies the paper on the *npj 2D Materials and Applications* website (doi:10.1038/s41699-017-0015-5).